

MULTI-WAVELENGTH COVERAGE OF STATE TRANSITIONS IN THE NEW BLACK HOLE X-RAY BINARY SWIFT J1910.2–0546

N. DEGENAAR^{1,8}, D. MAITRA^{1,2}, E.M. CACKETT³, M.T. REYNOLDS¹, J.M. MILLER¹, R.C. REIS^{1,9}, A.L. KING¹,
K.GÜLTEKIN¹, C.D. BAILYN⁴, M.M. BUXTON⁴, R.K.D. MACDONALD⁴, A.C. FABIAN⁵, D.B. FOX⁶, E.S. RYKOFF⁷

¹Department of Astronomy, University of Michigan, 500 Church Street, Ann Arbor, MI 48109, USA; degenaar@umich.edu

²Department of Physics and Astronomy, Wheaton College, 26 East Main Street, Norton, MA 02766, USA

³Department of Physics and Astronomy, Wayne State University, 666 West Hancock Street, Detroit, MI 48201, USA

⁴Astronomy Department, Yale University, P.O. Box 208101, New Haven, CT 06520-8101, USA

⁵Institute of Astronomy, University of Cambridge, Madingley Road, Cambridge CB3 0HA, UK

⁶Department of Astronomy and Astrophysics, Pennsylvania State University, 525 Davey Laboratory, University Park, PA 16802, USA

⁷SLAC National Accelerator Laboratory, Menlo Park, CA 94025, USA

Received 2013 November 28; accepted 2014 February 21

ABSTRACT

Understanding how black holes accrete and supply feedback to their environment is one of the outstanding challenges of modern astrophysics. Swift J1910.2–0546 is a candidate black hole low-mass X-ray binary that was discovered in 2012 when it entered an accretion outburst. To investigate the binary configuration and the accretion morphology we monitored the evolution of the outburst for $\simeq 3$ months at X-ray, UV, optical (B, V, R, I), and near-infrared (J, H, K) wavelengths using *Swift* and *SMARTS*. The source evolved from a hard to a soft X-ray spectral state with a relatively cold accretion disk that peaked at $\simeq 0.5$ keV. A *Chandra*/HETG spectrum obtained during this soft state did not reveal signatures of an ionized disk wind. Both the low disk temperature and the absence of a detectable wind could indicate that the system is viewed at relatively low inclination. The multi-wavelength light curves revealed two notable features that appear to be related to X-ray state changes. Firstly, a prominent flux decrease was observed in all wavebands $\simeq 1 - 2$ weeks before the source entered the soft state. This dip occurred in (0.6–10 keV) X-rays $\simeq 6$ days later than at longer wavelengths, which could possibly reflect the viscous time scale of the disk. Secondly, about two weeks after the source transitioned back into the hard state, the UV emission significantly increased while the X-rays steadily decayed. We discuss how these observations may reflect changes in the accretion morphology, perhaps related to the quenching/launch of a jet or the collapse/recovery of a hot flow.

Subject headings: accretion, accretion disks — black hole physics — ISM: jets and outflows — stars: individual (Swift J1910.2–0546) — X-rays: binaries

1. INTRODUCTION

Black holes in low-mass X-ray binaries (LMXBs) accrete matter from a low-mass ($\lesssim 1 M_{\odot}$) companion star that overflows its Roche lobe. During accretion outbursts, matter is supplied to the black hole through an accretion disk and outflows in the form of disk winds and jets are generated. X-ray monitoring has revealed a rich timing and spectral behavior leading to the formulation of distinct X-ray spectral states and transitions between them (e.g., Homan & Belloni 2005; Remillard & McClintock 2006).¹⁰

During *soft* states, the X-ray spectrum is dominated by thermal emission from the hot inner part of the accretion disk with a typical temperature of $kT_{\text{in}} \simeq 1$ keV (e.g., Dunn et al. 2011; Reynolds & Miller 2013). Strong ionized X-ray disk winds are commonly detected during this state (e.g., Miller et al. 2006; Ponti et al. 2012). In *hard* states, the accretion disk is colder and the X-ray spectrum is dominated by a power law with a photon index of $\Gamma \simeq 1.5 - 2$. Disk winds seem to be suppressed (e.g., Miller et al. 2008, 2012; Neilsen & Lee 2009), and in-

stead compact radio jets are observed (e.g., Fender et al. 2005). The hard X-rays are ascribed to a hot disk corona, a radiatively inefficient accretion flow, or a jet (e.g., Esin et al. 1997; Markoff et al. 2001; Brocksopp et al. 2004).

There are several mechanisms that are thought to contribute to the optical, ultraviolet (UV) and near-infrared (nIR) emission of black hole LMXBs. This radiation may originate in the cool outer parts of the accretion disk as the result of viscous dissipation or reprocessing of X-rays, but could also be produced in the jet, corona or inner hot flow (e.g., van Paradijs & McClintock 1995; Esin et al. 1997; Markoff et al. 2001; Russell et al. 2006; Rykoff et al. 2007; Veledina et al. 2011). The late-type companion star is typically dim and not contributing significantly to the outburst flux.

Multi-wavelength observations of the outburst evolution can shed light on the physical mechanisms producing the different emission components, the accretion inflow-outflow coupling, and the morphological changes occurring during X-ray state transitions. In this work we report on such a study of the newly discovered candidate black hole LMXB Swift J1910.2–0546.

2. SWIFT J1910.2–0546

Swift J1910.2–0546 (MAXI J1910–057) is a transient X-ray source that was discovered on 2012 May 30–

⁸ Hubble Fellow

⁹ Einstein Fellow

¹⁰ In this work we discuss X-ray spectral data in the 0.6–10 keV energy range and therefore we adopt a simplified soft/hard state nomenclature that neglects intermediate states.

31 through the monitoring surveys of *Swift*/BAT and *MAXI* (Krimm et al. 2012; Usui et al. 2012). An optical/nIR counterpart was readily identified and indicated an LMXB nature (Rau et al. 2012; Kennea et al. 2012). Initially, the optical emission was found to be highly variable, suggestive of a relatively short orbital period of $\simeq 2\text{--}4$ hr (Lloyd et al. 2012), but later spectroscopic studies favored a wider orbit of $\gtrsim 6.2$ hr (Casares et al. 2012). Apart from these estimates, no orbital ephemeris has been reported at present.

X-ray spectral analysis showed that the source traced out the canonical hard and soft states (Kennea et al. 2012; Kimura et al. 2012; Nakahira et al. 2012; Bodaghee et al. 2012; Reis et al. 2013), and a steady radio jet was detected (King et al. 2012). *Swift* J1910.2–0546 is therefore considered a new candidate black hole LMXB. X-ray reflection features detected with *XMM-Newton* suggested that the inner accretion disk may be truncated at a higher luminosity (i.e., a higher mass-accretion rate) than is typically seen in other black hole LMXBs, or alternatively could point to a retrograde spinning black hole (Reis et al. 2013).

3. OBSERVATIONS AND DATA ANALYSIS

Swift J1910.2–0546 is detected in the *Swift*/BAT and *MAXI* monitoring surveys for $\simeq 35$ weeks starting around MJD 56077 (2012 May 30).¹¹ We obtained contemporaneous X-ray, UV, optical and nIR monitoring observations between MJD 56140 and 56254 (2012 August 1 till November 23), using the *Swift* and *SMARTS* observatories. These observations sample $\simeq 3$ months of the full $\simeq 9$ -month outburst. We also obtained a *Chandra* observation to search for signatures of an ionized disk wind.

3.1. *Chandra* HETG Observation

Swift J1910.2–0546 was observed with *Chandra* for $\simeq 30$ ks starting on 2012 September 22 at UT 23:22 (MJD 56192, ObsID 14634). The incident flux was dispersed onto the ACIS-S CCDs using the High Energy Transmission Grating (HETG) with the ACIS-S array operated in the “CC33_GRADED” mode. The data were processed using the CIAO software (ver. 4.4). The positive and negative diffraction orders of the High-Energy Grating (HEG) and Medium-Energy Grating (MEG) spectra were combined using ADD_GRATING_ORDERS. The spectral data were fitted in XSPEC (ver. 12.7; Arnaud 1996).

3.2. *Swift* XRT and UVOT Observations

Swift J1910.2–0546 was monitored during 47 *Swift* observations of $\simeq 1$ ks that were performed between 2012 August 7 and November 23 (target ID 32521). These provide simultaneous coverage in X-rays and UV via the X-Ray Telescope (XRT) and the Ultra-Violet/Optical Telescope (UVOT), respectively. The *Swift* data were reduced using HEASOFT (ver. 6.13).

All XRT observations were carried out in Windowed Timing mode and processed using the task XRT_PIPELINE. The source was detected with raw XRT

¹¹ The *Swift*/BAT and *MAXI* light curves are consistent with the background level from 2013 January/February onward, although pointed *Swift*/XRT and ATCA radio observations indicated low-level accretion activity in 2013 May (Tomsick et al. 2013).

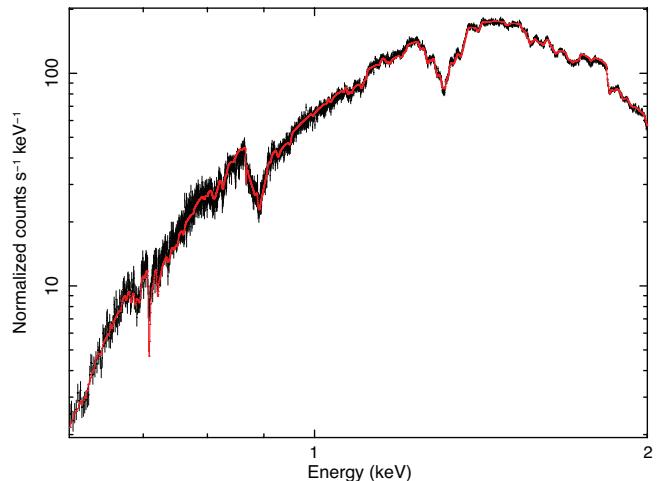


FIG. 1.— *Chandra*/MEG spectrum obtained during the soft state on MJD 56192 (2012 September 22). The red curve shows a fit using an absorbed disk black body. There are no X-ray absorption features that would testify to the presence of an ionized disk wind.

intensities varying between $\simeq 6$ and 250 counts s^{-1} . After examining the data for possible pile-up, we chose to conservatively exclude the central 3 pixels for count rates of $\simeq 150\text{--}200$ counts s^{-1} and 5 pixels for $\simeq 200\text{--}250$ counts s^{-1} (see also Reynolds & Miller 2013).

Using XSELECT, we extracted XRT spectra from a box of 60 pixels long and 20 pixels wide centered on the source. Background events were obtained from neighboring regions using a box of the same dimensions. The corresponding arfs were created using the tool XRTMKARF, and the rmfs (ver. 14) were sourced from the calibration data base. The spectral data were grouped to a minimum of 20 photons per bin. We also investigated the spectral evolution by determining the X-ray hardness ratio for each observation. For the purpose of the present work we defined this as the ratio of counts in the 1.5–10 keV and 0.6–1.5 keV energy bands.

All UVOT images were obtained using the *uvm2* filter ($\lambda_c \simeq 2246$ Å). Magnitudes and flux densities were extracted with the tool UVOTSOURCE using a standard aperture of $5''$. A nearby, source-free aperture of $15''$ served as a background reference.

3.3. *SMARTS* Optical and nIR Observations

We monitored *Swift* J1910.2–0546 at optical and nIR wavelengths using the ANDICAM detector mounted on the *SMARTS* 1.3-m telescope at the Cerro Tololo Inter-American Observatory in Chile. Between 2012 August 1 and October 17 the source was observed 42 times using a selection of *B*, *V*, *R*, *I*, *J*, *H*, and *K* filters.

Images of 250 s were obtained for the *B* and *V* filters, while the *R* and *I* band exposures were 300 s. The nIR data consisted of seven dithered images of 40 s each in *J*, seven dithered images of 40 s each in *H*, and thirteen dithered images of 25 s each in *K*. These dithered frames were flat-fielded, sky subtracted, aligned, and average-combined using an in-house IRAF script.

Two nearby 2MASS stars were taken as references to perform optical and nIR differential photometry with respect to *Swift* J1910.2–0546. Their optical magnitudes were taken from the NOMAD and USNO-B1 catalogs.

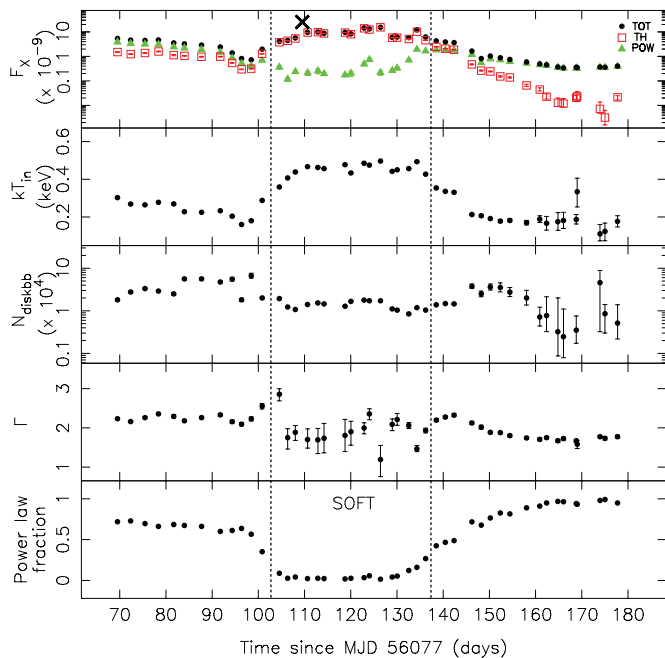


FIG. 2.— X-ray spectral evolution. From top to bottom: The 0.6–10 keV unabsorbed flux in units of 10^{-9} erg cm $^{-2}$ s $^{-1}$ (red squares for the disk, green triangles for the power law and black filled circles for the total flux), the inner disk temperature, the disk normalization, the power-law index, and the fractional contribution of the power law to the total flux. The “X” in the top panel marks the time of our *Chandra*/HETG observation. The vertical dotted lines illustrate when the source was in a soft state. Error bars represent 1σ confidence levels.

The night-to-night variability in the reference stars is accounted for in the magnitude errors.

4. RESULTS

4.1. No Sign of an Ionized Disk Wind

The *Chandra*/HETG observation was obtained during a soft state (see Section 4.2). However, the HEG and MEG spectra do not show X-ray absorption lines that would evidence the presence of an ionized disk wind (see Figure 1). We fitted the MEG data between 0.5 and 2.0 keV using an absorbed disk black body (DISKBB; Mitsuda et al. 1984) to constrain the hydrogen column density. For this purpose we adopted the TBNEW prescription with the VERN cross-sections and WILM abundances (Verner et al. 1996; Wilms et al. 2000).

The spectral fit shown in Figure 1 yielded a hydrogen column density of $N_H = (3.5 \pm 0.1) \times 10^{21}$ cm $^{-2}$, and a disk temperature of $kT_{in} = 0.42 \pm 0.01$ keV. Allowing the abundances of O, Ne, Mg and Fe to vary did not indicate any prominent deviations from Solar composition.

4.2. State Transitions and a Cool Disk

To obtain X-ray fluxes and to characterize the outburst evolution, all XRT spectra were fitted to a combined disk black body (DISKBB) and a power law (POWERLAW). Interstellar absorption was taken into account by using the TBABS model with the hydrogen column density fixed to $N_H = 3.5 \times 10^{21}$ cm $^{-2}$ (Section 4.1; for a justification, see Miller et al. 2009). X-ray fluxes were calculated in the 0.6–10 keV range. The results of our spectral analysis are illustrated in Figure 2.

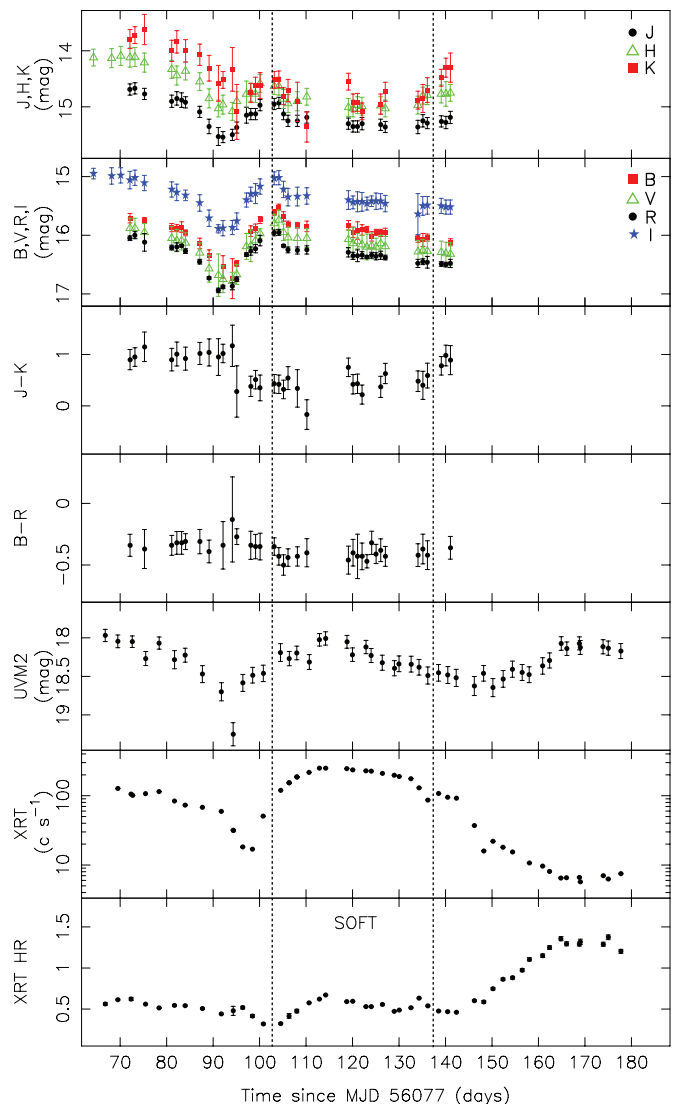


FIG. 3.— Multi-wavelength light curves and color evolution. From top to bottom: nIR, optical, nIR color, optical color, UV, 0.6–10 keV X-rays and X-ray hardness ratio (1.5–10 keV / 0.6–1.5 keV). The vertical dotted lines mark the time at which the source was in a soft state.

Our *Swift* observations started on 2012 August 7 (MJD 56146), shortly after Swift J1910.2–0546 had entered a hard state (Nakahira et al. 2012; Bodaghee et al. 2012; King et al. 2012). The XRT spectra were initially dominated by a hard power law with an index of $\Gamma \simeq 2$, but thermal emission from a relatively cool accretion disk with a temperature of $kT_{in} \simeq 0.25$ keV contributed $\simeq 40\%$ to the total 0.6–10 keV flux (Figure 2).¹²

Around September 5 (MJD 56175), the X-ray spectrum softened considerably. The disk temperature increased and the thermal emission dominated the 0.6–10 keV flux from September 10 onward (MJD 56180), indicating that Swift J1910.2–0546 had entered a soft state (Figure 2).¹³ Notably, even at the peak of the

¹² The relatively soft photon index and low hardness ratio suggests that the source may have been in an intermediate hard state at this time (see Figures 2 and 3).

¹³ The power-law index was not well constrained during the soft

soft state when the thermal emission accounted for $\simeq 99\%$ of the total flux, the disk remained relatively cool with $kT_{\text{in}} \simeq 0.5$ keV.

After October 2 (MJD 56202), the thermal flux started to decrease while the non-thermal flux increased. The disk cooled to a temperature of $kT_{\text{in}} \simeq 0.2$ keV and the power law hardened to $\Gamma \simeq 1.8$.¹⁴ During the last phase of our monitoring campaign (October 25 till November 23, MJD 56225–56254), the X-ray spectrum is completely dominated by the hard power law, demonstrating that the source was back in a hard state (Figure 2). Swift J1910.2–0546 thus traced out the typical black hole X-ray spectral states (see also Reis et al. 2013), and made two state transitions during our monitoring campaign.

4.3. Features in the Multi-wavelength Light Curves

Figure 3 displays the nIR, optical, UV and 0.6–10 keV X-ray light curves of Swift J1910.2–0546, as well as the evolution of the nIR (J – K) and optical (B – R) colors, and the X-ray hardness ratio. A striking feature is a dip in intensity that occurs $\simeq 95$ days into the outburst. At all wavelengths the flux steadily decreases toward a minimum on a time scale of $\simeq 10$ days, after which it recovers on a similar time scale. The optical and nIR magnitudes faded by $\simeq 0.9$ mag, which corresponds to a $\simeq 55\%$ drop in flux. The UV magnitude faded by $\simeq 1.3$ mag, or $\simeq 70\%$ in flux. The soft (disk) and hard (power law) X-ray flux decreased by $\simeq 80\%$ and 90% , respectively.

The measured X-ray flux reached a minimum on 2012 September 5 (MJD 56175; ObsID 32521012), whereas the point of lowest UV flux was recorded two observations earlier on September 1 (MJD 56171; ObsID 32521010). This is suggestive of a time delay between the different wavelengths (see also Krimm et al. 2013). In an attempt to quantify this delay, we fitted the light curves to a simple broken exponential to find the time of minimum flux in each band between August 23 and September 12 (days 85–105 in Figure 3). The results are listed in Table 1 and illustrated in Figure 4. Although the error margins are large, it appears that the dip first occurred in R , I , and J around day 92 (MJD 56169), whereas both longer (H and K) and shorter (B , V , and UV) wavelengths are delayed by $\simeq 1$ –4 days, followed by X-rays 6 days later (around day 98).

We also searched for and quantified any time lags using the standard cross-correlation analysis techniques widely used for optical reverberation in active galactic nuclei. We used a linear-interpolation cross correlation (White & Peterson 1994) and determined the uncertainties in the lags using a flux randomization and random subset sampling Monte Carlo method (Peterson et al. 1998, 2004). There were not enough points to apply this technique to a subset of the data covering the time of the flux dip only. Assuming that the variability in each waveband and each spectral state are caused by the same (or otherwise different but causally related) physical processes, we applied the method to the full data set. This

state because the hard flux contributed only $\simeq 1\%$ to the total 0.6–10 keV flux.

¹⁴ Even in the hardest spectra the addition of a soft component improves the fit over a single power law. For example, for the last observation (ObsID 32521049) adding a disk black body improves the fit from $\chi^2 = 274.93/236$ dof to $\chi^2 = 256.92/234$ dof with an f -test probability of $\simeq 3 \times 10^{-4}$.

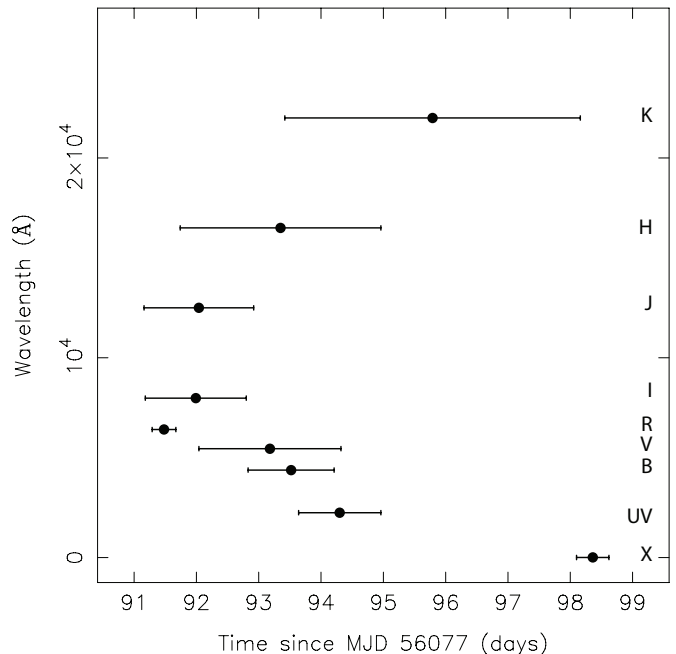


FIG. 4.— Time of minimum flux during the dip between MJD 56162–56182 (days 85–105) as measured in the different wavebands (indicated on the right).

analysis suggests that in the overall light curves there is a negligible time difference between the optical and nIR bands, but that the UV and X-rays lag the longer wavelengths by $\simeq 3$ and 8 days, respectively. These lags are not exactly the same as those estimated from the flux dip only (see Table 1), which may be the result of different emission mechanisms operating in the hard and soft spectral states.

Notably, Swift J1910.2–0546 entered a soft state $\simeq 1$ week after the intensity dip was seen in the X-rays (Section 4.2). This suggests a possible causal connection between the flux dip and the state transition (see Section 5). This is corroborated by the fact that around the time of the flux dip the nIR color suddenly became much bluer, e.g., the J – K color abruptly dropped from $\simeq 1$ to 0.5 around day 95 in Figure 3. In contrast, the optical bands continued to vary together, with little change in color, as illustrated by the evolution of B – R . The nIR colors remained blue during the soft state, only to become redder again when the H and K bands brightened and the source transitioned back into a hard state (around day 138; see also Section 5.3).

Whereas the *SMARTS* optical/nIR observations stopped at the end of the soft state, X-ray/UV monitoring with *Swift* continued. This revealed that the X-rays steadily decayed into the hard state, whereas the UV emission started to rise $\simeq 2$ weeks after the soft to hard state transition (around day 158). At the same time the X-ray spectrum considerably hardened, as illustrated by the strong increase in XRT hardness ratio (Figure 3).

4.4. Relation between the X-Ray and UV Flux

To investigate the apparent anti-correlation seen between the UV and X-rays in the hard state (Section 4.3), we calculated UV fluxes ($F_{\text{uv}m2}$) by multiplying the measured UVOT flux densities with the FWHM of the *uvm2*

TABLE 1
TIME LAGS IN SWIFT J1910.2–0546.

Waveband	Lag (days)	
	Flux Dip	Full Light Curve
UV–X-ray	4.06 ± 0.71	$7.72^{+0.80}_{-0.71}$
B–X-ray	4.84 ± 0.74	8.24 ± 0.43
B–UV	0.78 ± 0.95	$2.72^{+1.00}_{-0.58}$
B–V	-0.34 ± 1.33	-0.13 ± 0.26
B–R	-2.04 ± 0.72	-0.52 ± 0.18
B–I	-1.53 ± 1.06	-0.52 ± 0.22
B–J	-1.48 ± 1.12	$-0.38^{+0.28}_{-0.24}$
B–H	-0.17 ± 1.75	$-0.13^{+0.49}_{-0.44}$
B–K	2.27 ± 2.47	...

NOTE. — The waveband listed first is taken as the reference, i.e., the lag given is with respect to that. When considering the full light curve no lag could be determined for the K band, as it was poorly correlated with the other light curves.

filter ($\simeq 498$ Å; Poole et al. 2008). In Figure 5 we plot the relation between the UV and the 0.6–10 keV X-ray flux. Above $F_X \simeq 10^{-9}$ erg cm $^{-2}$ s $^{-1}$, the two are positively correlated (Spearman rank coefficient $\rho = 0.52$, corresponding to a $\simeq 3\sigma$ significance), whereas at lower fluxes a very significant negative correlation is apparent ($\rho = 0.96$; $\simeq 7\sigma$).

To quantify these relations, we fitted both sides separately to a power law of the form $F_{\text{uv}2} \propto F_X^\beta$. This yielded $\beta = 0.15 \pm 0.05$ and -0.45 ± 0.03 for the positive and negative correlation, respectively (dotted lines in Figure 5). A fit with a broken power law yields similar indices ($\beta \simeq 0.22$ and -0.45), and a break located at $F_X \simeq 1.1 \times 10^{-9}$ erg cm $^{-2}$ s $^{-1}$.

To investigate the time evolution along the X-ray/UV relations, we divided the outburst into five contiguous intervals of 9/10 observations: These are indicated by different symbols in Figure 5. This illustrates that the UV/X-ray relation evolved from a positive into a negative correlation once the source had moved from the soft to the hard state (around day 138). The anti-correlation thus mostly arises during the last part of the light curves when the UV emission rises while the X-rays decrease (Figure 3).

It is plausible that the observed anti-correlation is introduced due to the presence of a time lag between the X-ray and UV emission. To gauge this possibility, we investigated the relation after applying a time lag of 7.72 days (Section 4.3). Figure 5 (right) shows that a negative correlation arising from the last set of observations persists, although it is less significant ($\rho = 0.68$; $\simeq 2\sigma$). The positive correlation is now stronger ($\rho = 0.59$; $\simeq 4\sigma$). A fit with a broken power law yields the same indices as before applying the time lag ($\beta \simeq 0.15$ and -0.45), and a break located at $F_X \simeq 7 \times 10^{-10}$ erg cm $^{-2}$ s $^{-1}$.

The observed (anti-) correlation is thus sensitive to the presence of a time lag. We determined a 7.72 days time delay between the X-ray and UV emission using the full light curves. However, since different emission mechanisms could be contributing to the UV flux in the hard and soft spectral states, different delays may be expected and hence affecting the observed X-ray/UV relation (see also Section 5.3). We note that the *Swift*/BAT

and *MAXI* monitoring light curves show that the outburst of Swift J1910.2–0546 continued after our pointed XRT and UVOT observations stopped (due to Sun constraints). The X-ray/UV relation may have eventually returned to a positive correlation, tracing out a similar path as the X-ray/nIR relation seen in other black holes (e.g., Coriat et al. 2009). However, it is not clear if the underlying physical processes should be the same.

5. DISCUSSION

5.1. Inclination and Disk Temperature

A *Chandra*/HETG spectrum obtained when Swift J1910.2–0546 was in the soft state appeared featureless, despite the fact that ionized disk winds are expected to be ubiquitous in this spectral state (e.g., Miller et al. 2008, 2012). If such winds are mostly equatorial, a possible explanation for the lack of ionized absorption features is that Swift J1910.2–0546 is viewed at relatively low inclination (Ponti et al. 2012). This would be consistent with the analysis of disk reflection features, which suggested an inclination of $i \lesssim 20^\circ$ (Reis et al. 2013).

Geometrical effects could also account for the fact that the accretion disk of Swift J1910.2–0546 peaked at $kT_{\text{in}} \simeq 0.5$ keV, which is much cooler than typically seen for black hole LMXBs in the soft state ($kT_{\text{in}} \gtrsim 1$ keV; e.g., Dunn et al. 2011; Reynolds & Miller 2013). As shown by Muñoz-Darias et al. (2013), disks look cooler when viewed at lower inclination, which can be understood in terms of relativistic effects. Swift J1910.2–0546 could thus fit into this picture. Alternatively, the low temperature could be the result of a small disk size, e.g., due to a short orbital period (see Section 5.2), a truncated disk or a retrograde black hole spin (Reis et al. 2013).

5.2. Viscous Time Scale of the Accretion Disk?

Our multi-wavelength light curves revealed a prominent flux dip that first appeared in the optical band, only to be followed by X-rays $\simeq 6$ days later. A comparable X-ray lag ($\simeq 8$ days) is suggested by cross-correlating the light curves over the full time range covered by our monitoring campaign. A natural explanation for the observed delay may be a (small-scale) mass-transfer instability that originated at the outer edge of the accretion disk and then propagated inward. The time delay could then represent the viscous time scale of the disk, $t_{\text{visc}}(r) = \frac{2}{3\alpha} \left(\frac{h}{r}\right)^{-2} \Omega_K^{-1}$. Here α is the viscosity parameter, h the scale height of the disk, and Ω_K the Keplerian frequency at radius r .

Assuming $\alpha = 0.1$, $h/r = 0.01$ (i.e., a geometrically thin disk), and $M = 8 M_\odot$, a viscous time scale of $t_{\text{visc}} = 6$ days would yield a disk radius of $r \simeq 3400 GM/c^2$ ($\simeq 4 \times 10^9$ cm). This is relatively small, perhaps supporting the fairly short $\simeq 2$ – 4 hr orbital period hinted by its rapid optical flaring (Lloyd et al. (2012), but see Casares et al. (2012)). On the other hand, a comparable time delay of several days between the nIR and X-rays has also been inferred for black hole LMXBs that have (much) longer orbital periods (e.g., LMC–X3, GX 339–4, and 4U 1957+11; Brocksopp et al. 2001; Homan et al. 2005; Russell et al. 2010).

The interpretation of the dip as a mass-transfer instability could naturally explain why in all bands the flux recovered to the pre-dip level. However, this picture may

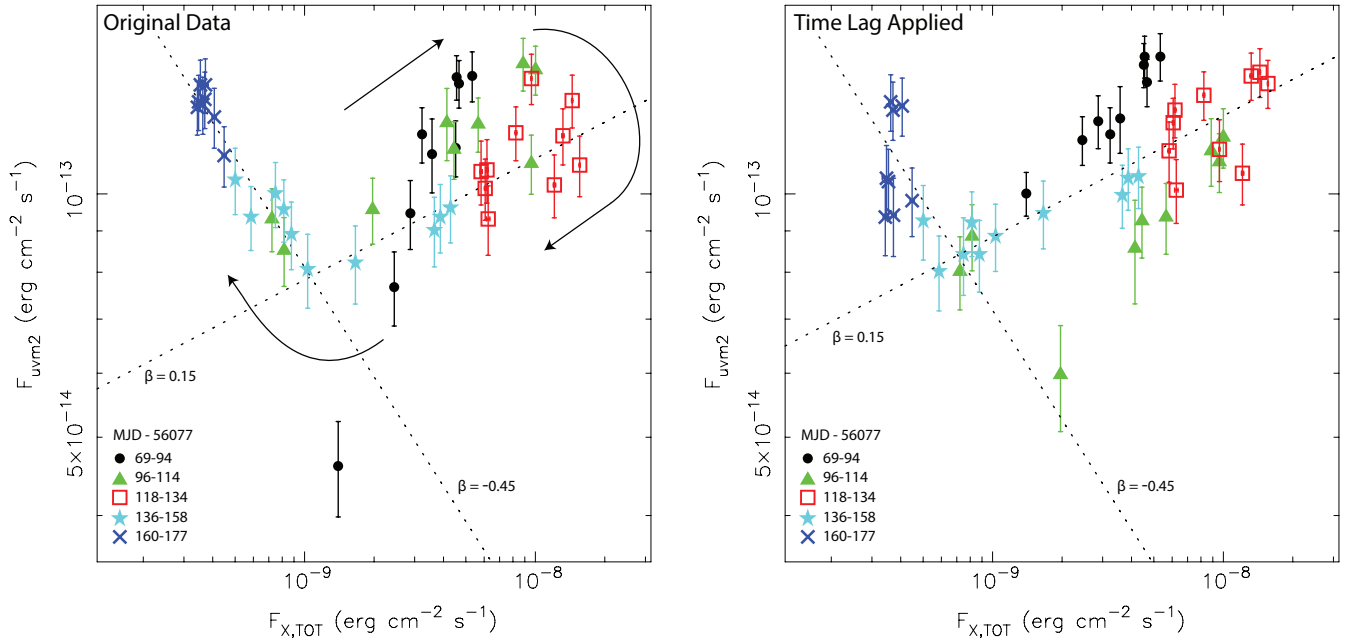


FIG. 5.— Relation between the *Swift* X-ray and UV fluxes. Dotted lines indicate fits to a power law of the form $F_{\text{uv}2} \propto F_X^\beta$. The temporal evolution is encoded in the different symbols, which indicate the time in days since MJD 56077 (arrows are indicated to guide the eye). The right plot illustrates how the relation changes after applying a time delay of 7.72 days for the X-rays with respect to the UV.

not account for the fact that the flux appeared to hit a minimum in the *H* and *K* bands later than in the optical/UV (albeit still before the X-rays; Figure 4). This may suggest that multiple (competing) emission mechanisms are operating, or that the flux dip is the result of a different physical process altogether (Section 5.3). This is perhaps hinted by the fact that there appears to be a causal connection between the dip and the transition to the soft state $\simeq 1 - 2$ weeks later. This connection would not be obvious to explain in terms of a small-scale mass-transfer instability.

5.3. Changes in the Accretion Flow Morphology

Interestingly, a very similar flux dip as we observed for Swift J1910.2–0546 was reported for GX 339–4 during its 2010 outburst (Yan & Yu 2012). In that source the UV flux decreased by $\simeq 60\%$ in $\simeq 2$ weeks time, which was associated with a drop in the optical/nIR (by $\simeq 85\%$) as well as the radio flux. Within $\simeq 10$ days after this drop the source transitioned from a hard to soft state, and the UV flux dip was therefore associated with jet quenching (Yan & Yu 2012).

In Swift J1910.2–0546, support for change in accretion morphology (perhaps connected to a jet) is provided the observation that the nIR color suddenly became bluer right around the time of the flux dip (Figure 3). It remained as such until the end of the soft state, which started $\simeq 10$ days after the color change. This behavior was not observed in the optical bands, suggesting a relative suppression of the nIR emission during the soft state, i.e., when jets are known to be quenched.

When the source transitioned back to the hard state, the *K* and *H* band flux started to rise and the nIR color become redder again (around day 138 in Figure 3). Although our *SMARTS* monitoring stopped at this time, the hinted nIR brightening may be similar to that seen

in other black hole LMXBs entering the hard state (e.g., Jain et al. 2001; Buxton & Bailyn 2004; Buxton et al. 2012; Kalemci et al. 2005, 2013; Russell et al. 2010, 2013; Dinger et al. 2012; Corbel et al. 2013). The optical/nIR secondary maxima seen in these sources have been ascribed to the revival of a jet (e.g., Dinger et al. 2012; Kalemci et al. 2013).

Continued *Swift* monitoring revealed that in Swift J1910.2–0546 the UV emission started to increase $\simeq 20$ days after the transition back into the hard state (around day 158 in Figure 3), whereas the X-rays continuously decayed. This caused the relation between the UV and 0.6–10 keV flux to move from a positive correlation (with a slope of $\beta \simeq 0.15$) into a negative correlation ($\beta \simeq -0.45$). This turnover in the UV/X-ray relation occurred at $F_X \simeq 10^{-9}$ erg cm $^{-2}$ s $^{-1}$ (0.6–10 keV). The distance toward Swift J1910.2–0546 is unknown, but if the peak of the outburst (as observed by *MAXI*) did not exceed the Eddington limit (L_{EDD}), the transition flux corresponds to $\lesssim 0.03 \times L_{\text{EDD}}$. The UV brightening was accompanied by a dramatic increase in the X-ray hardness ratio, which again suggests a causal connection with changes in the accretion morphology.

This rise in UV emission is reminiscent of the secondary nIR/optical maxima seen in other black hole LMXBs. In a systematic study of a number of different sources and outbursts, Kalemci et al. (2013) showed that the nIR peaks $\simeq 5 - 15$ days after the transition from the soft to the hard state. In Swift J1910.2–0546, the UV appears to peak $\simeq 10$ days after it starts rising, or $\simeq 30$ days after the state transition (around day 168 in Figure 3). This is thus considerably later than the reported nIR peaks (Kalemci et al. 2013). In a jet interpretation it might be expected that the UV increases after the nIR (Corbel et al. 2013; Russell et al. 2013), but it is not immediately clear if this delay could be as large

as $\simeq 20$ days.

An alternative interpretation for both the multi-wavelength flux dip and the UV peak may be provided in terms of the collapse and recovery of a hot inner flow (Veledina et al. 2011, 2013). Such a radiatively inefficient flow might replace the inner accretion disk at low mass-accretion rates (e.g., Esin et al. 1997). Analysis of disk reflection features suggested that the disk in Swift J1910.2–0546 could indeed be subject to evaporation (Reis et al. 2013). This model predicts that the outer regions of the hot flow (traced by the optical/nIR emission) collapses several days before an X-ray state transition is observed (causing a decrease in flux; Veledina et al. 2013). This is consistent with the time between the dip and the soft state transition observed for Swift J1910.2–0546 ($\simeq 1$ –2 weeks). Moreover, the hot flow model predicts that the optical/nIR spectrum hardens (i.e., becomes bluer) in this transition, consistent with the drop in $J - K$ color that we observed before the state transition (Figure 3).

Veledina et al. (2011) interpret the optical/nIR secondary maxima seen after hard state transitions as the recovery of a hot inner flow (see also Kalemci et al. 2013; Veledina et al. 2013). The same mechanism may account for the UV peak (and corresponding X-ray/UV anti-correlation) discussed in this work. However, in the picture of a recovering hot flow, the UV emission should rise before the nIR (Veledina et al. 2013), whereas in Swift J1910.2–0546 there are indications that the nIR started to rise first. Moreover, a delay as long as $\simeq 30$ days between the state transition and the UV peak may be difficult to account for (see also Kalemci et al. 2013).

It is worth noting that although UV monitoring is

often hampered by substantial interstellar extinction, anti-correlated UV and X-ray emission has also been observed for the neutron star Cyg X-2 (Rykoff et al. 2010). On the other hand, such an anti-correlation was not seen for the black hole LMXBs XTE J1817–330 and Swift J1357.2–0933, despite dense UV/X-ray coverage over a large range of fluxes (Rykoff et al. 2007; Armas Padilla et al. 2013). The latter source may have never entered a soft state (Armas Padilla et al. (2013), see also Corral-Santana et al. (2013) and Shahbaz et al. (2013)), which could possibly explain the absence of an anti-correlation given that the UV rise appears to be connected to a state transition. However, XTE J1817–330 was monitored for well over a month after it transitioned from the soft to the hard state, but its X-ray and UV emission remained tightly correlated (Rykoff et al. 2007). Future X-ray/UV monitoring efforts of suitable targets are warranted to further understand the role of the UV emission in state transitions.

The authors are grateful to the anonymous referee for constructive and insightful comments that helped improve this manuscript. N.D. is supported by NASA through Hubble Postdoctoral Fellowship grant number HST-HF-51287.01-A from the Space Telescope Science Institute. R.C.R. is supported by NASA through the Einstein fellowship program (grant number PF1-120087) and is a member of the Michigan Society of Fellows. J.M.M. gratefully acknowledges support from the Swift guest observer program. N.D. thanks A. Veledina, J. Poutanen, and M. van Dijk for stimulating discussions.

Facilities: CXO (HETG), CTIO:1.3m, Swift (XRT,UVOT)

REFERENCES

- Armas Padilla, M., Degenaar, N., Russell, D. M., & Wijnands, R. 2013, *MNRAS*, 428, 3083
- Arnaud, K. A. 1996, in *Astronomical Society of the Pacific Conference Series*, Vol. 101, *Astronomical Data Analysis Software and Systems V*, ed. G. H. Jacoby & J. Barnes, 17
- Bodaghee, A., Bozzo, E., Tomsick, J. A., et al. 2012, *ATel*, 4328
- Brocksopp, C., Bandyopadhyay, R. M., & Fender, R. P. 2004, *New Astronomy*, 9, 249
- Brocksopp, C., Groot, P. J., & Wilms, J. 2001, *MNRAS*, 328, 139
- Buxton, M. M., & Bailyn, C. D. 2004, *ApJ*, 615, 880
- Buxton, M. M., Bailyn, C. D., Capelo, H. L., et al. 2012, *AJ*, 143, 130
- Casares, J., Rodríguez-Gil, P., Zurita, C., et al. 2012, *ATel*, 4347
- Corbel, S., Aassel, H., Broderick, J. W., et al. 2013, *MNRAS*, 431, L107
- Coriat, M., Corbel, S., Buxton, M. M., et al. 2009, *MNRAS*, 400, 123
- Corral-Santana, J. M., Casares, J., Muñoz-Darias, T., et al. 2013, *Science*, 339, 1048
- Dinçer, T., Kalemci, E., Buxton, M. M., et al. 2012, *ApJ*, 753, 55
- Dunn, R. J. H., Fender, R. P., Körding, E. G., Belloni, T., & Merloni, A. 2011, *MNRAS*, 411, 337
- Esin, A. A., McClintock, J. E., & Narayan, R. 1997, *ApJ*, 489, 865
- Fender, R., Belloni, T., & Gallo, E. 2005, *Ap&SS*, 300, 1
- Homan, J., & Belloni, T. 2005, *Ap&SS*, 300, 107
- Homan, J., Buxton, M., Markoff, S., et al. 2005, *ApJ*, 624, 295
- Jain, R. K., Bailyn, C. D., Orosz, J. A., McClintock, J. E., & Remillard, R. A. 2001, *ApJ*, 554, L181
- Kalemci, E., Dinçer, T., Tomsick, J. A., et al. 2013, *ApJ*, 779, 95
- Kalemci, E., Tomsick, J. A., Buxton, M. M., et al. 2005, *ApJ*, 622, 508
- Kennea, J. A., Krimm, H. A., & Holland, S. T. 2012, *ATel*, 4149
- Kimura, M., Tomida, H., Nakahira, S., et al. 2012, *ATel*, 4198
- King, A. L., Miller, J. M., Degenaar, N., Reynolds, M., & Reis, R. 2012, *ATel*, 4295
- Krimm, H. A., Barthelmy, S. D., Baumgartner, W., et al. 2012, *ATel*, 4139
- Krimm, H. A., Holland, S. T., Corbet, R. H. D., et al. 2013, *ApJS*, 209, 14
- Lloyd, C., Oksanen, A., Starr, P., Darlington, G., & Pickard, R. 2012, *ATel*, 4246
- Markoff, S., Falcke, H., Yuan, F., & Biermann, P. L. 2001, *A&A*, 379, L13
- Miller, J. M., Cackett, E. M., & Reis, R. C. 2009, *ApJ*, 707, L77
- Miller, J. M., Raymond, J., Reynolds, C. S., et al. 2008, *ApJ*, 680, 1359
- Miller, J. M., Raymond, J., Homan, J., et al. 2006, *ApJ*, 646, 394
- Miller, J. M., Raymond, J., Fabian, A. C., et al. 2012, *ApJ*, 759, L6
- Mitsuda, K., Inoue, H., Koyama, K., et al. 1984, *PASJ*, 36, 741
- Muñoz-Darias, T., Coriat, M., Plant, D. S., et al. 2013, *MNRAS*, 432, 1330
- Nakahira, S., Ueda, Y., Takagi, T., et al. 2012, *ATel*, 4273
- Neilsen, J., & Lee, J. C. 2009, *Nature*, 458, 481
- Peterson, B. M., Wanders, I., Bertram, R., et al. 1998, *ApJ*, 501, 82
- Peterson, B. M., Ferrarese, L., Gilbert, K. M., et al. 2004, *ApJ*, 613, 682
- Ponti, G., Fender, R. P., Begelman, M. C., et al. 2012, *MNRAS*, 422, L11
- Poole, T. S., Breeveld, A. A., Page, M. J., et al. 2008, *MNRAS*, 383, 627
- Rau, A., Greiner, J., & Schady, P. 2012, *ATel*, 4144
- Reis, R. C., Reynolds, M. T., Miller, J. M., et al. 2013, *ApJ*, 778, 155
- Remillard, R. A., & McClintock, J. E. 2006, *ARA&A*, 44, 49
- Reynolds, M. T., & Miller, J. M. 2013, *ApJ*, 769, 16
- Russell, D. M., Fender, R. P., Hynes, R. I., et al. 2006, *MNRAS*, 371, 1334
- Russell, D. M., Maitra, D., Dunn, R. J. H., & Markoff, S. 2010, *MNRAS*, 405, 1759
- Russell, D. M., Russell, T. D., Miller-Jones, J. C. A., et al. 2013, *ApJ*, 768, L35
- Rykoff, E. S., Cackett, E. M., & Miller, J. M. 2010, *ApJ*, 719, 1993

- Rykoff, E. S., Miller, J. M., Steeghs, D., & Torres, M. A. P. 2007, *ApJ*, 666, 1129
- Shahbaz, T., Russell, D. M., Zurita, C., et al. 2013, *MNRAS*, 434, 2696
- Tomsick, J. A., Corbel, S., Rodriguez, J., & Tzioumis, T. 2013, *ATel*, 5063
- Usui, R., Nakahira, S., Tomida, H., et al. 2012, *ATel*, 4140
- van Paradijs, J., & McClintock, J. E. 1995, in *X-ray binaries*, p. 58 - 125, ed. W. H. G. Lewin, J. van Paradijs, & E. P. J. van den Heuvel, 58–125
- Veledina, A., Poutanen, J., & Vurm, I. 2011, *ApJ*, 737, L17
- . 2013, *MNRAS*, 430, 3196
- Verner, D. A., Ferland, G. J., Korista, K. T., & Yakovlev, D. G. 1996, *ApJ*, 465, 487
- White, R. J., & Peterson, B. M. 1994, *PASP*, 106, 879
- Wilms, J., Allen, A., & McCray, R. 2000, *ApJ*, 542, 914
- Yan, Z., & Yu, W. 2012, *MNRAS*, 427, L11